

Analyst

Accepted Manuscript

This article can be cited before page numbers have been issued, to do this please use: F. Ravera, E. Efeoglu and H. J. Byrne, *Analyst*, 2025, DOI: 10.1039/D4AN01509F.



This is an Accepted Manuscript, which has been through the Royal Society of Chemistry peer review process and has been accepted for publication.

Accepted Manuscripts are published online shortly after acceptance, before technical editing, formatting and proof reading. Using this free service, authors can make their results available to the community, in citable form, before we publish the edited article. We will replace this Accepted Manuscript with the edited and formatted Advance Article as soon as it is available.

You can find more information about Accepted Manuscripts in the [Information for Authors](#).

Please note that technical editing may introduce minor changes to the text and/or graphics, which may alter content. The journal's standard [Terms & Conditions](#) and the [Ethical guidelines](#) still apply. In no event shall the Royal Society of Chemistry be held responsible for any errors or omissions in this Accepted Manuscript or any consequences arising from the use of any information it contains.

Monitoring the Kinetic Evolution of Mesenchymal Stem Cell Differentiation using Raman Microspectroscopy

F. Ravera¹, E. Efeoglu², H.J. Byrne¹

¹ FOCAS Research Institute, Technological University Dublin, City Campus, Dublin 8, Ireland

² National Institute for Cellular Biotechnology (NICB), Dublin City University, Dublin 9, Ireland

Corresponding Author: Francesca Ravera (D16126527@mytudublin.ie)

Abstract

Raman microspectroscopy (RMS) offers a powerful, non-destructive approach for *in situ* monitoring of dynamic biochemical processes within cells. However, the ability to reliably data-mine the spectroscopic signatures and their evolution and extract meaningful information can be challenging. Multivariate Curve Resolution-Alternating Least Squares (MCR-ALS) regression analysis is a powerful chemometric technique that can potentially address this challenge by deconvoluting the spectra into individual component spectra, each representing a specific biochemical species, and regressing the solutions against kinetic constraints.

In this study, MCR-ALS analysis was performed on spectral data of differentiation process of mesenchymal stem cells into chondrocytes, carried out on two different substrates, collagen 3-dimensional hydrogel and the conventional 2-dimensional culture model at time intervals of 1-7, 14, 21 days. The kinetic evolution of the chondrogenesis was modelled according to a phenomenological rate equation model, in an attempt to describe the biochemical evolution of the cell composition within the process. Moreover, the ability of the algorithm to faithfully extract the correct reaction rates and spectral profiles has been explored. The results indicated that the differentiation process originates in the nucleolar regions, subsequently extending to

the nuclear and cytoplasmic compartments and corroborated a more rapid differentiation rate in cell cultures grown on 3D collagen hydrogels compared to 2D substrates.

The combination of Raman microspectroscopy and MCR-ALS offers a powerful approach for elucidating the complex mechanisms underlying chondrogenesis and developing innovative strategies for regenerative medicine.

Keywords: Raman spectroscopy, mesenchymal stem cells, chondrogenesis, kinetic evolution, Multivariate Curve Resolution-Alternating Least Squares regression analysis

1. Introduction

Cell therapy is a rapidly emerging field of regenerative medicine that involves the injection or implantation of living cells into a patient to treat a variety of diseases and injuries [1]. By leveraging the body's inherent healing mechanisms, cell therapies aim to restore damaged tissues and organs. The development of cell-based therapies, particularly those employing stem cells, holds significant promise for regenerative medicine. However, to realise the full potential of these therapies, a comprehensive understanding of cellular behaviour and function is essential. This necessitates the development of robust monitoring methods that can track cell-based therapies throughout their entire lifecycle, from initial cell isolation to clinical application. Such monitoring can enable researchers and clinicians to optimise culture conditions, ensure product quality, and assess safety and efficacy [1].

Within the context of stem cell-based therapies, a particular focus lies on chondrogenesis, the process of cartilage formation from mesenchymal stem cells (MSCs) [2]. Chondrocytes play a pivotal role in the maintenance of cartilage through the secretion of growth factors and enzymes that regulate its synthesis and extracellular matrix (ECM) [3]. Chondrogenesis is regulated by multiple complex signalling paths, and, during the first phase of intense growth, known as pre-cartilaginous condensation, MSCs cluster together and become a flock of mesenchymal progenitor cells and nodules [3-5]. This pre-cartilaginous condensation is an extremely

1
2
3 important intermediate phase that provides the fundamental scaffold for the skeletal elements, and it is provoked by a reduction of intercellular distances and consequent increase of cell to
4
5
6
7
8 cell contacts [3]. Within these densely packed cellular aggregates, the MSCs further
9
10
11
12
13 differentiate into chondrocytes, which proliferate and continue the deposition of extracellular
14
15
16 matrix [3, 5].

17
18
19
20
21
22
23
24
25
26
27
28
29
30
31
32
33
34
35
36
37
38
39
40
41
42
43
44
45
46
47
48
49
50
51
52
53
54
55
56
57
58
59
60
61
62
63
64
65
66
67
68
69
70
71
72
73
74
75
76
77
78
79
80
81
82
83
84
85
86
87
88
89
90
91
92
93
94
95
96
97
98
99
100
101
102
103
104
105
106
107
108
109
110
111
112
113
114
115
116
117
118
119
120
121
122
123
124
125
126
127
128
129
130
131
132
133
134
135
136
137
138
139
140
141
142
143
144
145
146
147
148
149
150
151
152
153
154
155
156
157
158
159
160
161
162
163
164
165
166
167
168
169
170
171
172
173
174
175
176
177
178
179
180
181
182
183
184
185
186
187
188
189
190
191
192
193
194
195
196
197
198
199
200
201
202
203
204
205
206
207
208
209
210
211
212
213
214
215
216
217
218
219
220
221
222
223
224
225
226
227
228
229
230
231
232
233
234
235
236
237
238
239
240
241
242
243
244
245
246
247
248
249
250
251
252
253
254
255
256
257
258
259
260
261
262
263
264
265
266
267
268
269
270
271
272
273
274
275
276
277
278
279
280
281
282
283
284
285
286
287
288
289
290
291
292
293
294
295
296
297
298
299
300
301
302
303
304
305
306
307
308
309
310
311
312
313
314
315
316
317
318
319
320
321
322
323
324
325
326
327
328
329
330
331
332
333
334
335
336
337
338
339
340
341
342
343
344
345
346
347
348
349
350
351
352
353
354
355
356
357
358
359
360
361
362
363
364
365
366
367
368
369
370
371
372
373
374
375
376
377
378
379
380
381
382
383
384
385
386
387
388
389
390
391
392
393
394
395
396
397
398
399
400
401
402
403
404
405
406
407
408
409
410
411
412
413
414
415
416
417
418
419
420
421
422
423
424
425
426
427
428
429
430
431
432
433
434
435
436
437
438
439
440
441
442
443
444
445
446
447
448
449
450
451
452
453
454
455
456
457
458
459
460
461
462
463
464
465
466
467
468
469
470
471
472
473
474
475
476
477
478
479
480
481
482
483
484
485
486
487
488
489
490
491
492
493
494
495
496
497
498
499
500
501
502
503
504
505
506
507
508
509
510
511
512
513
514
515
516
517
518
519
520
521
522
523
524
525
526
527
528
529
530
531
532
533
534
535
536
537
538
539
540
541
542
543
544
545
546
547
548
549
550
551
552
553
554
555
556
557
558
559
560
561
562
563
564
565
566
567
568
569
570
571
572
573
574
575
576
577
578
579
580
581
582
583
584
585
586
587
588
589
590
591
592
593
594
595
596
597
598
599
600
601
602
603
604
605
606
607
608
609
610
611
612
613
614
615
616
617
618
619
620
621
622
623
624
625
626
627
628
629
630
631
632
633
634
635
636
637
638
639
640
641
642
643
644
645
646
647
648
649
650
651
652
653
654
655
656
657
658
659
660
661
662
663
664
665
666
667
668
669
670
671
672
673
674
675
676
677
678
679
680
681
682
683
684
685
686
687
688
689
690
691
692
693
694
695
696
697
698
699
700
701
702
703
704
705
706
707
708
709
710
711
712
713
714
715
716
717
718
719
720
721
722
723
724
725
726
727
728
729
730
731
732
733
734
735
736
737
738
739
740
741
742
743
744
745
746
747
748
749
750
751
752
753
754
755
756
757
758
759
760
761
762
763
764
765
766
767
768
769
770
771
772
773
774
775
776
777
778
779
780
781
782
783
784
785
786
787
788
789
790
791
792
793
794
795
796
797
798
799
800
801
802
803
804
805
806
807
808
809
810
811
812
813
814
815
816
817
818
819
820
821
822
823
824
825
826
827
828
829
830
831
832
833
834
835
836
837
838
839
840
841
842
843
844
845
846
847
848
849
850
851
852
853
854
855
856
857
858
859
860
861
862
863
864
865
866
867
868
869
870
871
872
873
874
875
876
877
878
879
880
881
882
883
884
885
886
887
888
889
890
891
892
893
894
895
896
897
898
899
900
901
902
903
904
905
906
907
908
909
910
911
912
913
914
915
916
917
918
919
920
921
922
923
924
925
926
927
928
929
930
931
932
933
934
935
936
937
938
939
940
941
942
943
944
945
946
947
948
949
950
951
952
953
954
955
956
957
958
959
960
961
962
963
964
965
966
967
968
969
970
971
972
973
974
975
976
977
978
979
980
981
982
983
984
985
986
987
988
989
990
991
992
993
994
995
996
997
998
999
1000
1001
1002
1003
1004
1005
1006
1007
1008
1009
1010
1011
1012
1013
1014
1015
1016
1017
1018
1019
1020
1021
1022
1023
1024
1025
1026
1027
1028
1029
1030
1031
1032
1033
1034
1035
1036
1037
1038
1039
1040
1041
1042
1043
1044
1045
1046
1047
1048
1049
1050
1051
1052
1053
1054
1055
1056
1057
1058
1059
1060
1061
1062
1063
1064
1065
1066
1067
1068
1069
1070
1071
1072
1073
1074
1075
1076
1077
1078
1079
1080
1081
1082
1083
1084
1085
1086
1087
1088
1089
1090
1091
1092
1093
1094
1095
1096
1097
1098
1099
1100
1101
1102
1103
1104
1105
1106
1107
1108
1109
1110
1111
1112
1113
1114
1115
1116
1117
1118
1119
1120
1121
1122
1123
1124
1125
1126
1127
1128
1129
1130
1131
1132
1133
1134
1135
1136
1137
1138
1139
1140
1141
1142
1143
1144
1145
1146
1147
1148
1149
1150
1151
1152
1153
1154
1155
1156
1157
1158
1159
1160
1161
1162
1163
1164
1165
1166
1167
1168
1169
1170
1171
1172
1173
1174
1175
1176
1177
1178
1179
1180
1181
1182
1183
1184
1185
1186
1187
1188
1189
1190
1191
1192
1193
1194
1195
1196
1197
1198
1199
1200
1201
1202
1203
1204
1205
1206
1207
1208
1209
1210
1211
1212
1213
1214
1215
1216
1217
1218
1219
1220
1221
1222
1223
1224
1225
1226
1227
1228
1229
1230
1231
1232
1233
1234
1235
1236
1237
1238
1239
1240
1241
1242
1243
1244
1245
1246
1247
1248
1249
1250
1251
1252
1253
1254
1255
1256
1257
1258
1259
1260
1261
1262
1263
1264
1265
1266
1267
1268
1269
1270
1271
1272
1273
1274
1275
1276
1277
1278
1279
1280
1281
1282
1283
1284
1285
1286
1287
1288
1289
1290
1291
1292
1293
1294
1295
1296
1297
1298
1299
1300
1301
1302
1303
1304
1305
1306
1307
1308
1309
1310
1311
1312
1313
1314
1315
1316
1317
1318
1319
1320
1321
1322
1323
1324
1325
1326
1327
1328
1329
1330
1331
1332
1333
1334
1335
1336
1337
1338
1339
1340
1341
1342
1343
1344
1345
1346
1347
1348
1349
1350
1351
1352
1353
1354
1355
1356
1357
1358
1359
1360
1361
1362
1363
1364
1365
1366
1367
1368
1369
1370
1371
1372
1373
1374
1375
1376
1377
1378
1379
1380
1381
1382
1383
1384
1385
1386
1387
1388
1389
1390
1391
1392
1393
1394
1395
1396
1397
1398
1399
1400
1401
1402
1403
1404
1405
1406
1407
1408
1409
1410
1411
1412
1413
1414
1415
1416
1417
1418
1419
1420
1421
1422
1423
1424
1425
1426
1427
1428
1429
1430
1431
1432
1433
1434
1435
1436
1437
1438
1439
1440
1441
1442
1443
1444
1445
1446
1447
1448
1449
1450
1451
1452
1453
1454
1455
1456
1457
1458
1459
1460
1461
1462
1463
1464
1465
1466
1467
1468
1469
1470
1471
1472
1473
1474
1475
1476
1477
1478
1479
1480
1481
1482
1483
1484
1485
1486
1487
1488
1489
1490
1491
1492
1493
1494
1495
1496
1497
1498
1499
1500
1501
1502
1503
1504
1505
1506
1507
1508
1509
1510
1511
1512
1513
1514
1515
1516
1517
1518
1519
1520
1521
1522
1523
1524
1525
1526
1527
1528
1529
1530
1531
1532
1533
1534
1535
1536
1537
1538
1539
1540
1541
1542
1543
1544
1545
1546
1547
1548
1549
1550
1551
1552
1553
1554
1555
1556
1557
1558
1559
1560
1561
1562
1563
1564
1565
1566
1567
1568
1569
1570
1571
1572
1573
1574
1575
1576
1577
1578
1579
1580
1581
1582
1583
1584
1585
1586
1587
1588
1589
1590
1591
1592
1593
1594
1595
1596
1597
1598
1599
1600
1601
1602
1603
1604
1605
1606
1607
1608
1609
1610
1611
1612
1613
1614
1615
1616
1617
1618
1619
1620
1621
1622
1623
1624
1625
1626
1627
1628
1629
1630
1631
1632
1633
1634
1635
1636
1637
1638
1639
1640
1641
1642
1643
1644
1645
1646
1647
1648
1649
1650
1651
1652
1653
1654
1655
1656
1657
1658
1659
1660
1661
1662
1663
1664
1665
1666
1667
1668
1669
1670
1671
1672
1673
1674
1675
1676
1677
1678
1679
1680
1681
1682
1683
1684
1685
1686
1687
1688
1689
1690
1691
1692
1693
1694
1695
1696
1697
1698
1699
1700
1701
1702
1703
1704
1705
1706
1707
1708
1709
1710
1711
1712
1713
1714
1715
1716
1717
1718
1719
1720
1721
1722
1723
1724
1725
1726
1727
1728
1729
1730
1731
1732
1733
1734
1735
1736
1737
1738
1739
1740
1741
1742
1743
1744
1745
1746
1747
1748
1749
1750
1751
1752
1753
1754
1755
1756
1757
1758
1759
1760
1761
1762
1763
1764
1765
1766
1767
1768
1769
1770
1771
1772
1773
1774
1775
1776
1777
1778
1779
1780
1781
1782
1783
1784
1785
1786
1787
1788
1789
1790
1791
1792
1793
1794
1795
1796
1797
1798
1799
1800
1801
1802
1803
1804
1805
1806
1807
1808
1809
1810
1811
1812
1813
1814
1815
1816
1817
1818
1819
1820
1821
1822
1823
1824
1825
1826
1827
1828
1829
1830
1831
1832
1833
1834
1835
1836
1837
1838
1839
1840
1841
1842
1843
1844
1845
1846
1847
1848
1849
1850
1851
1852
1853
1854
1855
1856
1857
1858
1859
1860
1861
1862
1863
1864
1865
1866
1867
1868
1869
1870
1871
1872
1873
1874
1875
1876
1877
1878
1879
1880
1881
1882
1883
1884
1885
1886
1887
1888
1889
1890
1891
1892
1893
1894
1895
1896
1897
1898
1899
1900
1901
1902
1903
1904
1905
1906
1907
1908
1909
1910
1911
1912
1913
1914
1915
1916
1917
1918
1919
1920
1921
1922
1923
1924
1925
1926
1927
1928
1929
1930
1931
1932
1933
1934
1935
1936
1937
1938
1939
1940
1941
1942
1943
1944
1945
1946
1947
1948
1949
1950
1951
1952
1953
1954
1955
1956
1957
1958
1959
1960
1961
1962
1963
1964
1965
1966
1967
1968
1969
1970
1971
1972
1973
1974
1975
1976
1977
1978
1979
1980
1981
1982
1983
1984
1985
1986
1987
1988
1989
1990
1991
1992
1993
1994
1995
1996
1997
1998
1999
2000
2001
2002
2003
2004
2005
2006
2007
2008
2009
2010
2011
2012
2013
2014
2015
2016
2017
2018
2019
2020
2021
2022
2023
2024
2025
2026
2027
2028
2029
2030
2031
2032
2033
2034
2035
2036
2037
2038
2039
2040
2041
2042
2043
2044
2045
2046
2047
2048
2049
2050
2051
2052
2053
2054
2055
2056
2057
2058
2059
2060
2061
2062
2063
2064
2065
2066
2067
2068
2069
2070
2071
2072
2073
2074
2075
2076
2077
2078
2079
2080
2081
2082
2083
2084
2085
2086
2087
2088
2089
2090
2091
2092
2093
2094
2095
2096
2097
2098
2099
2100
2101
2102
2103
2104
2105
2106
2107
2108
2109
2110
2111
2112
2113
2114
2115
2116
2117
2118
2119
2120
2121
2122
2123
2124
2125
2126
2127
2128
2129
2130
2131
2132
2133
2134
2135
2136
2137
2138
2139
2140
2141
2142
2143
2144
2145
2146
2147
2148
2149
2150
2151
2152
2153
2154
2155
2156
2157
2158
2159
2160
2161
2162
2163
2164
2165
2166
2167
2168
2169
2170
2171
2172
2173
2174
2175
2176
2177
2178
2179
2180
2181
2182
2183
2184
2185
2186
2187
2188
2189
2190
2191
2192
2193
2194
2195
2196
2197
2198
2199
2200
2201
2202
2203
2204
2205
2206
2207
2208
2209
2210
2211
2212
2213
2214
2215
2216

are often destructive, time-consuming, and require large sample quantities [10, 22-30], limiting their clinical and translational applications [10, 22-30].

Vibrational spectroscopy can overcome numerous limitations and has been extensively explored over the last decades as a diagnostic and prognostic tool for biomedical applications [31, 32]. Raman microspectroscopy (RMS), has previously been used to provide an *in situ* and real time assessment of stem cell quality and differentiation potential [29, 33, 34].

Expanding upon the work of Ravera *et al.* (2024) on the benefits of 3D hydrogels compared to conventional 2D cell culture for *in vitro* chondrogenesis, this study aims to investigate and quantitatively compare the kinetic evolution and different rates of differentiation of MSCs on different substrates. In this work, it is proposed that the different stages of chondrocyte development, from undifferentiated MSCs to pre-chondrogenic condensed cells, and early differentiated chondrocytes, respectively, can be represented by distinct spectral profiles identified in the Raman spectral profile of the cell population. The kinetics of the evolution process can thus be modelled according to a phenomenological rate equation model, in which a series of ordinary differential equations are used to describe the biochemical evolution of the cell composition from their undifferentiated state, through pre-chondrogenic condensation to differentiated chondrocytes. The kinetic model will then be used as a set of constraints applied to the multivariate curve resolution- alternating least squares (MCR-ALS) algorithm to extract the independent spectral profiles (Components) from the measured spectra as a function of time, as well as kinetic rate constants to characterise the differentiation process [35].

MCR-ALS regression analysis is an unmixing method which can provide an accurate molecular decomposition of the spectroscopic information contained in a data set [35, 36]. The algorithm operates under the assumption that any given complex spectrum within the analysis can be represented as a linear combination of pure component spectra. These components are weighted based on their relative abundance at each point in the analysis. Within the context of

MCR-ALS image analysis, a "pure component" can represent a singular chemical compound or a distinct stage within a process that exhibits a consistent spectral signature [35-37]. MCR-ALS is rapidly emerging as a powerful tool for spectral analysis, offering valuable insights. Perez-Guaita *et al.* previously used MCR-ALS combined with pharmacokinetic modelling to analyse the uptake of drugs by cells *in vitro*. This approach allowed them to extract the spectral signatures and concentration profiles of the drug and its metabolites over time [38]. Moreover, MCR-ALS has been applied for innovative analysis of skin tissues, providing *in vivo* spectral profiles corresponding to the contribution of the optical system and skin components [39]. By utilising MCR-ALS to analyse the kinetic evolution the differentiation process, according to a model of $A \rightarrow B$, $B \rightarrow C$, with rate constants of k_1 and k_2 , respectively, this study aims to extract the underlying spectral components and their corresponding concentration profiles from the Raman spectra of MSCs cultured on both 2D and 3D hydrogel substrates and moreover quantify the process in terms of the rate constants of the progression. This approach will enable a detailed analysis of the progressive evolution of the spectral features associated with the different phases of chondrogenesis, including the initial condensation of MSCs, the subsequent differentiation into chondrocytes, and the maturation of the extracellular matrix. Furthermore, this study will focus on the subcellular localisation of spectral changes, examining the evolution of the organelles quantitatively comparing the kinetic profiles of these subcellular regions in MSCs differentiated on 2D and 3D substrates, quantifying their rates of change, providing valuable insights into the influence of the microenvironment on the chondrogenic process.

Overall, this study leverages the power of MCR-ALS to unravel the complex spectral signatures of MSCs undergoing chondrogenesis, offering a deeper understanding of the molecular and cellular mechanisms involved in this critical developmental process, and

demonstrating the potential of Raman microspectroscopy as a tool for monitoring the development of cell-based therapies.

2. Materials and Methods

2.1. Summary

The manuscript presents a further analysis of the spectral data previously presented in Ravera *et al.* [33, 40]. For completeness, the Materials and Methods of that study are summarised here. Briefly, rat mesenchymal stem cells (rMSCs) from GIBCO® (Thermo Fisher Scientific) were cultured in Dulbecco's Modified Eagle Medium (DMEM) supplemented with 10% foetal bovine serum (FBS) and 5 µg/mL gentamicin. Sub-culturing was performed every 3-4 days at 60-80% confluency to maintain a healthy and expanding cell population. As a well studied model for the differentiation process, a commercially available rodent mesenchymal stem cell line was chosen. Chondrogenic differentiation has previously been demonstrated by positive proteoglycan Alcian blue staining after 18 days of culturing [12, 41], and by monitoring the content of sulphated glycosaminoglycans after 14, 21 and 28 days [18, 42, 43]. To induce chondrogenesis, a commercially available StemPro™ Chondrogenesis Differentiation Kit (Thermo Fisher Scientific) was employed. The comparison of two distinct culture environments was carried out, 3D and 2D, for 3 weeks. 3D cell cultures were prepared according to previously described protocol [40] with collagen hydrogel-coated dishes (Collagen I, rat tail (3 mg/mL) GIBCO®) and seeded with rMSCs at a density of 5×10^6 cells/mL. 2D cell cultures were seeded onto polystyrene plates at a density of 8×10^6 cells/mL and then seeded onto CaF₂ disks (Crystran, UK) at a specific density of 100,000 cells per disk for Raman analysis. All samples were fixed with 10% formalin solution, rinsed with and stored in distilled water (dH₂O) for Raman measurements.



2.2. Raman Spectral Data

For Raman analysis of rMSCs, control and differentiated cultures, samples were prepared by directly fixing the samples with formaldehyde solution. Cells were washed three times with Dulbecco's Phosphate-Buffered Saline (D-PBS, containing no calcium, magnesium, or phenol red), then fixed with 10% formalin for 15 minutes. The formalin solution was removed after 15 minutes of incubation at room temperature, cells were rinsed with dH₂O three times and kept in 2 mL of dH₂O for Raman measurements.

A Horiba Jobin-Yvon LabRAM HR800 spectrometer, equipped with a 785 nm diode laser as source, was used throughout the study. All measurements were acquired in water to reduce scatter and minimise the risk of photodamage [44, 45], by using a x100 water immersion objective (LUMPlanF1, Olympus, N.A. 1), of spot size ~1 μm. The spectrometer was calibrated to the 520.7 cm⁻¹ line of silicon prior to spectral acquisition. Although the high resolution HR800 instrument can achieve a dispersion of ~0.25 cm⁻¹ per pixel with higher density gratings, 300 lines per mm grating was chosen to capture the whole fingerprint region of the spectrum in a single window, with a spectral dispersion of approximately 1.5 cm⁻¹ per pixel. A 100 μm confocal pinhole was used for all measurements. The spectra were dispersed onto a 16-bit dynamic range Peltier cooled CCD detector and the spectral range from 400 to 1800 cm⁻¹, the so-called fingerprint region, was chosen. Point spectra from the cytoplasm, nucleus, and nucleolus (See Figure S.1.) of 20 to 40 cells were acquired for each differentiation time point, and spectra were acquired for 3 x 30 seconds at each spot.

2.3. Spectral Data Processing

Prior to analysis, raw spectral data underwent pre-processing in Matlab (Mathworks) to remove unwanted background signal and noise. A Savitzky-Golay filter (3rd order, 9 points) was applied to smooth the spectra. The background signal, primarily water due to immersion

1
2
3
4
5
6
7
8
9
10
11
12
13
14
15
16
17
18
19
20
21
22
23
24
25
26
27
28
29
30
31
32
33
34
35
36
37
38
39
40
41
42
43
44
45
46
47
48
49
50
51
52
53
54
55
56
57
58
59
60

geometry [45, 46], was removed using the adapted Extended Multiplicative Signal Correction (EMSC) algorithm [47]. EMSC was applied to the smoothed spectra using a reference spectrum of cells on collagen hydrogel and a 7th-order polynomial baseline. Finally, the data was vector normalised to minimise instrumental variation. Each dataset contained 20-40 spectra (observations), representing points in an n-dimensional space defined by the wavenumbers (400-1800 cm^{-1}).

2.4. Multivariate Curve Resolution-Alternating Least Squares Modelling

Multivariate Curve Resolution-Alternating Least Squares (MCR-ALS) was performed to resolve the multiple component responses within the measured spectral responses, as explained in detail by de Juan and Tauler [37].

The MCR-ALS Graphical User Interface (GUI) 2.0 was employed for all analyses presented in this study [37, 48]. It is freely available from the Multivariate Curve Resolution Homepage (<https://mcrals.wordpress.com/>). The GUI was run in Matlab 2023b (Mathworks). Singular Value Decomposition was used to initially specify the number of components as 3. Initial estimates of the components were then performed using Evolving Factor Analysis. The fitting procedure was subjected to non-negativity (NNLS) constraints in both the concentration and spectral domains, and no further normalisation was applied. Kinetic constraints of $A \rightarrow B \rightarrow C$ were applied to the concentration domain, 100 iterations were performed, and the convergence criterion was set at 0.01.

Following the definition of the kinetic model across the specified time frame (t_1 to t_n), the program performs an optimisation routine, resulting in the generation of the best-fit kinetic profiles for component concentrations (c_{opt}) and their corresponding spectral profiles (s_{opt}). Notably, the optimised kinetic parameters are also recorded for each model variation, such as those arising from adjustments to the time window or time step.

3. Results and Discussion

View Article Online
DOI: 10.1039/D4AN01509F

3.1. Tracking Subcellular Biochemical Changes in MSC Differentiation with Raman microspectroscopy and MCR-ALS

Raman microspectroscopic analysis was performed on the subcellular regions of nucleolus, nucleus and cytoplasm of rMSC cultures in both 2D and 3D environments, over a period of 1-21 days [33, 40].

MCR-ALS was initially used to examine the spectral information gathered from Raman microspectroscopy of subcellular regions of differentiating MSCs towards chondrocytes cultured and differentiated on collagen hydrogel substrates. Singular value decomposition (SVD) was used to first establish the number of components to be used in the model, which was specified as 3, imposing a three-stage model of initial differentiation from rMSC (A) to the condensation stage (B), followed by the last differentiation stage (C), on the evolution of the Raman spectra of the nucleolus over the 21 days of differentiation. The resultant spectral components can be seen in Figure 1.A, for the case of the nucleoli. The kinetic evolution of the components, constrained to an evolution model of $A \rightarrow B, B \rightarrow C$, with rate constants of k_1 and k_2 (per day), respectively, can be seen in Figure 1.B. The fit parameters are tabulated in Table 1. To better visualise the spectroscopic changes occurring between the stages, the difference spectra (Component 2- Component 1) and (Component 3- Component 2), are shown in Figure 1.C.

A difference spectrum is a visual representation of the calculated difference between two spectra, obtained by subtracting one spectrum from the other, point by point. Difference spectra are particularly useful for highlighting subtle changes that might be difficult to discern when comparing the original spectra directly. They can also help identify changes in peaks and visualise the level of differences between spectra. Additionally, difference spectra can reveal

the main peaks of the spectra being compared, as these peaks will often appear as prominent features in the difference spectrum.

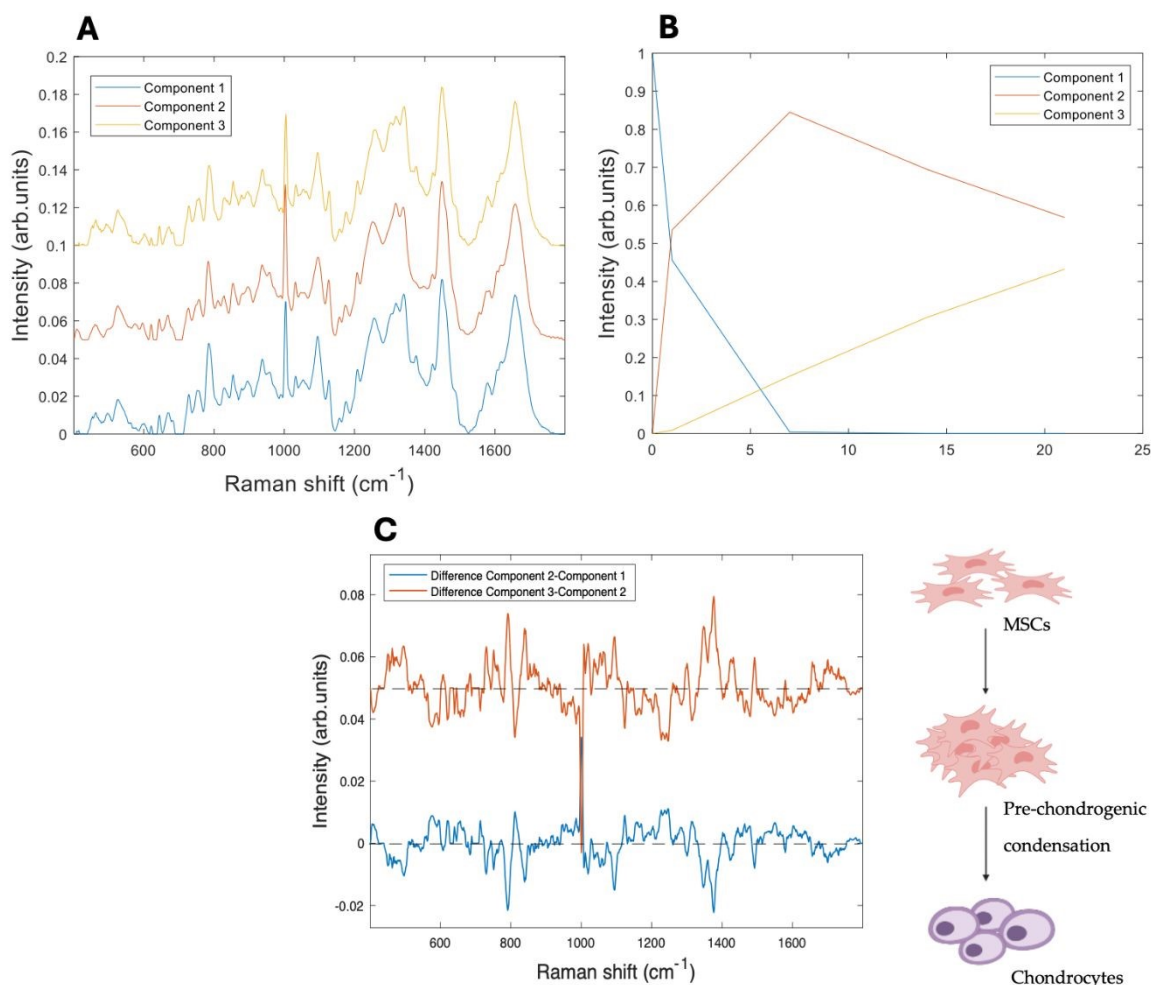


Figure 1. **A)** MCR-ALS resolved components corresponding to the evolution of the nucleolus over a 21 day period of differentiation on 3D collagen I hydrogels (offset for clarity). **B)** Three stage kinetic model of the evolution of the kinetic components $A \rightarrow B$, $B \rightarrow C$. **C)** Difference spectra between the first and the second component (blue) and second and third (red) (offset for clarity). The dashed lines indicate zero difference.

View Article Online
DOI: 10.1039/D4AN01509F

		3D				2D			
		k1	k2	Sig	Sig 2	k1	k2	Sig	Sig 2
A → B B → C				1				1	
	Nucleolus	0.47	0.04	0.05	0.00	0.25	0.04	0.01	0.00
	Nucleus	0.22	0.02	0.03	0.00	0.12	0.05	0.01	0.00
	Cytoplasm	1.19	0.23	0.16	0.03	0.15	0.04	0.01	0.00
B → C		0.16		0.02					

Table 1. Optimised rate constants (per day) of kinetic equations $A \rightarrow B$ (k_1) and $B \rightarrow C$ (k_2) for each of the three subcellular regions of cells grown in 2-dimensional and 3-dimensional substrates (2D and 3D). Sig 1 and Sig 2 indicate the residual standard deviation for k_1 and k_2 , respectively.

Component 1 is seen to decrease dramatically after one day of differentiation, while component 2 increases concomitantly and continues to dominate throughout 21 days of differentiation. Component 3 shows a steady increase throughout the differentiation process, although it only accounts for ~40% of the spectral profile after 21 days. As expected, the main spectral changes observed in the nucleolus (figure 1.A) from Components 1 to 3 are associated with nucleic acid structures, including an increased intensity of the phosphate stretching vibration of RNA/DNA content, such as the band at $\sim 782\text{-}86\text{ cm}^{-1}$, manifest as a sharp peak, compared to the other components [49].

Figure 1.C illustrates the difference spectra between the three components and allows a clearer identification of the spectral changes occurring between the stages of the differentiation process. The peak at $\sim 1093\text{ cm}^{-1}$, corresponding to the stretching vibration of RNA/DNA, is present in the spectral representation of both difference spectra [50], and there are further changes in the DNA/RNA related peak at $\sim 1336\text{ cm}^{-1}$ [51]. However, further significant changes are also observed in the intensities of protein and lipid related peaks, for example the peak at $\sim 1004\text{ cm}^{-1}$, assigned to phenylalanine [52], and the range of $1303\text{--}1343\text{ cm}^{-1}$, in which the most relevant peaks (1303 cm^{-1} , 1322 cm^{-1} and 1343 cm^{-1}) correspond to the contribution of CH_2CH_3 bending in collagen [53]. Changes are also observed at the peaks at $\sim 1123\text{ cm}^{-1}$ (C-C stretching mode of lipids and proteins), $\sim 1453\text{ cm}^{-1}$, and $\sim 1468\text{ cm}^{-1}$ (CH bending mode of structural proteins and lipids) [54].

An intense nucleolar activity in the early phases of differentiation, or pre-chondrogenic condensation, has previously been observed with Raman microspectroscopy [33, 55] and indicates that the nucleolus is the primary site of biochemical activity in the initial stages of differentiation [56, 57]. This decrease is closely linked to a reduction in transcriptional activity and cell proliferation, as stem cells transition from a highly proliferative state to a more specialised, functionally distinct phenotype [29, 33, 55].

This intense activity is reflected in the changes occurring in Component 2 in the first days of the differentiation of the pure components analysis with MCR-ALS. Interestingly, many of the spectral changes evident in the difference spectrum representing the first phase of differentiation appear to be reversed in the second phase, as evidenced by the almost mirror image nature of the second difference spectrum.

Further significant changes are also observed in the intensities of protein and lipid related peaks, for example the peak at $\sim 1004\text{ cm}^{-1}$, assigned to phenylalanine [52], and the range of $1303\text{--}1343\text{ cm}^{-1}$, in which the most relevant peaks (1303 cm^{-1} , 1322 cm^{-1} and 1343 cm^{-1})

correspond to the contribution of CH_2CH_3 bending in collagen [53]. Changes are also observed at the peaks at $\sim 1123 \text{ cm}^{-1}$ (C-C stretching mode of lipids and proteins), $\sim 1453 \text{ cm}^{-1}$, and $\sim 1468 \text{ cm}^{-1}$ (CH bending mode of structural proteins and lipids) [54]. During chondrogenic differentiation a decrease in sphingomyelins and phosphatidylcholines has previously been detected [58]. Lipid changes are crucial for differentiation progression, and the identified markers could aid in monitoring chondrogenesis and improving cartilage regeneration. The findings emphasise the role of lipids in cell growth, differentiation, and cartilage matrix production.

To further explore the effectiveness of MCR-ALS analysis, a comparative study of the spectroscopic results of rMSCs chondrogenic differentiation analysis performed on cells grown on a 2-D CaF_2 was performed. The equivalent plot for the analysis of the datasets for the nucleolus, nucleus and cytoplasm in a 2D environment are shown in the Supplementary material Figures S.2.-S.4. The results showed interesting similarities and differences when compared with the equivalent data obtained on different growth substrate but otherwise, the same differentiation conditions.

Interestingly, the rate of differentiation from undifferentiated rMSCs towards the pre-chondrogenic phase ($k_1 = 0.47 \pm 0.05$ per day) appears higher on a 3D hydrogel substrate than the equivalent observed organelle grown onto a 2D substrate ($k_1 = 0.25 \pm 0.01$ per day) (Table 1). However, the rate of differentiation from the second to the third component k_2 is significantly lower ($k_2 = 0.040 \pm 0.003$ per day) on the 3D substrate, and a similar value is observed for the equivalent process on 2D ($k_2 = 0.04 \pm 0.002$ per day).



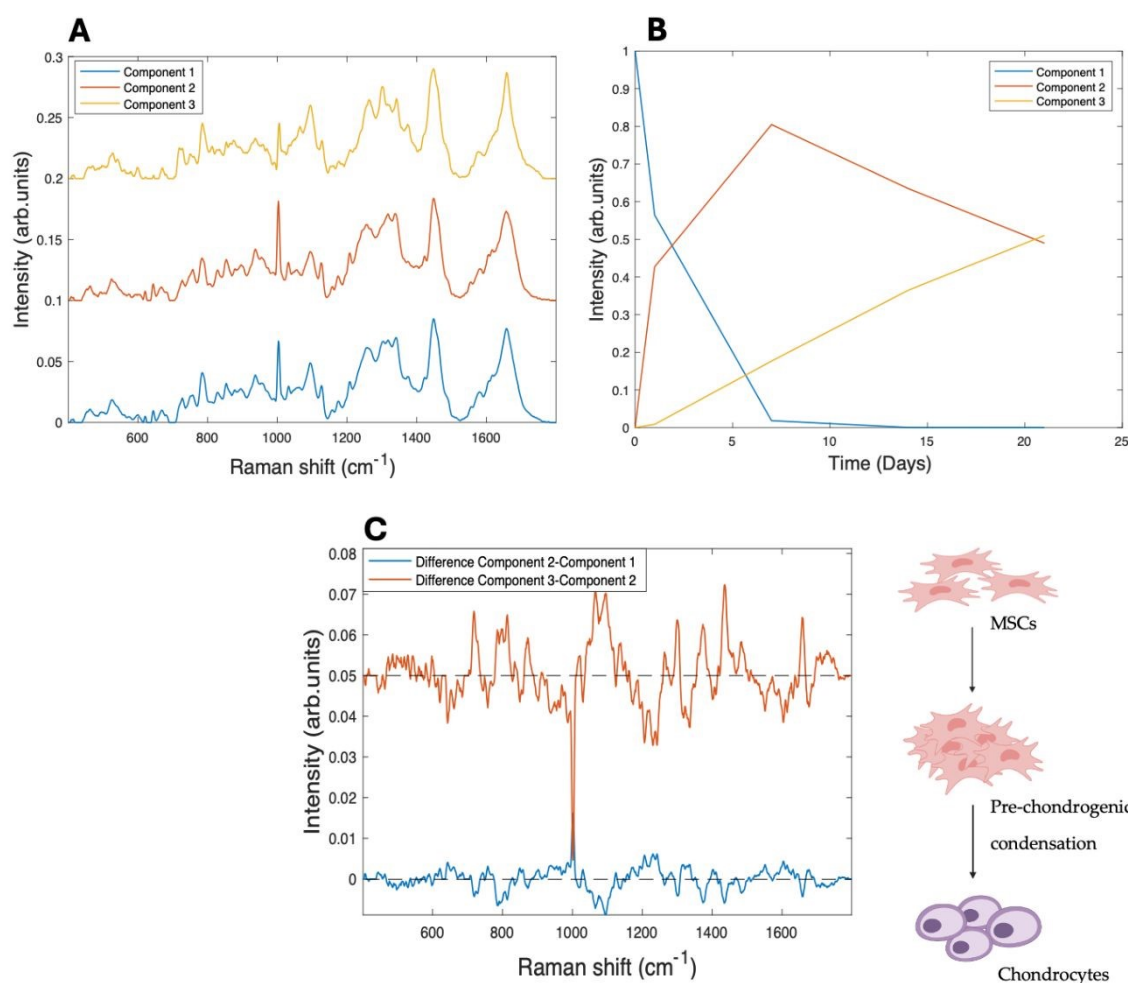


Figure 2. **A)** MCR-ALS resolved components corresponding to the evolution of the nucleus over a 21 day period of differentiation on 3D collagen I hydrogels, offset for clarity. **B)** Three stage kinetic model of the evolution of the kinetic components $A \rightarrow B$, $B \rightarrow C$. **C)** Difference spectra between the first and the second component (blue) and second and third (red), offset for clarity. The dashed lines indicate zero difference.

A similar analysis was performed on the nucleus, and the spectral profiles and their kinetic evolution are shown in figure 2.A&B and the difference spectra in figure 2.C. In terms of the

1
2
3 evolution kinetics, Component 1 is again seen to have completely decayed by day 7, while
4
5 Component 2 still represents ~50% of the spectral profile after 21 days (figure 2.B). Similarly
6
7 to the nucleolus, as differentiation progresses, the increase of Component 2 (from day 1
8
9 onwards) represents the development of the pre-chondrogenic condensation phase, in which
10
11 intense transcriptional activity is known to occur [4, 59]. This is further supported by the
12
13 observed increase in peaks associated with RNA/DNA content (786 cm^{-1} , 1093 cm^{-1}) within
14
15 component B [49]. However, the difference spectra between components of the nucleus present
16
17 distinctive features compared to the equivalent nucleolar spectra. Firstly, it appears that the
18
19 main molecular changes take place between the second and third component, and therefore in
20
21 the second phase of the differentiation. This is manifested in the difference spectrum Figure
22
23 3.C (red), in which more prominent peaks associated with relevant spectral changes are
24
25 observable, while the spectrum generated by the difference between the first and the second
26
27 components (blue) shows fewer remarkable peaks.

28
29 The main changes are observed in the range $\sim 1300\text{-}1340\text{ cm}^{-1}$ which shows differences of
30
31 intensity similar to those observed for the nucleolus. Other peaks are attributable to the
32
33 contribution of nucleic acids of DNA/RNA (1263 cm^{-1} , $\sim 1342\text{ cm}^{-1}$), $\text{CH}_2\text{CH}_3\text{ cm}^{-1}$ of collagen
34
35 ($1300\text{-}1304\text{ cm}^{-1}$), and $1318\text{-}1337\text{ cm}^{-1}$ (DNA/RNA and Amide III) [60].

36
37 Interestingly, peaks at $\sim 1004\text{ cm}^{-1}$ (assigned to phenylalanine), 1064 cm^{-1} – 1088 cm^{-1} C-O, C-
38
39 C stretching (carbohydrates) show a prominent increase, potentially reflecting changes in
40
41 protein and GAGs synthesis associated with the formation of the chondrogenic extracellular
42
43 matrix [61, 62].

44
45 As is the case for the nucleolus, the comparison with the nuclear spectral data obtained onto
46
47 2D substrate reveals a higher kinetic constant k_1 of the cell culture on 3D than on 2D ($3\text{D}=0.22$
48
49 ± 0.02 per day and $2\text{D}=0.12 \pm 0.01$ per day). In this case, however, the rate of the second phase,
50
51
52
53
54
55
56
57
58
59
60

k₂, appears to be higher on the 2D substrate (3D=0.025 ± 0.003 per day and 2D=0.052 ± 0.006 per day).

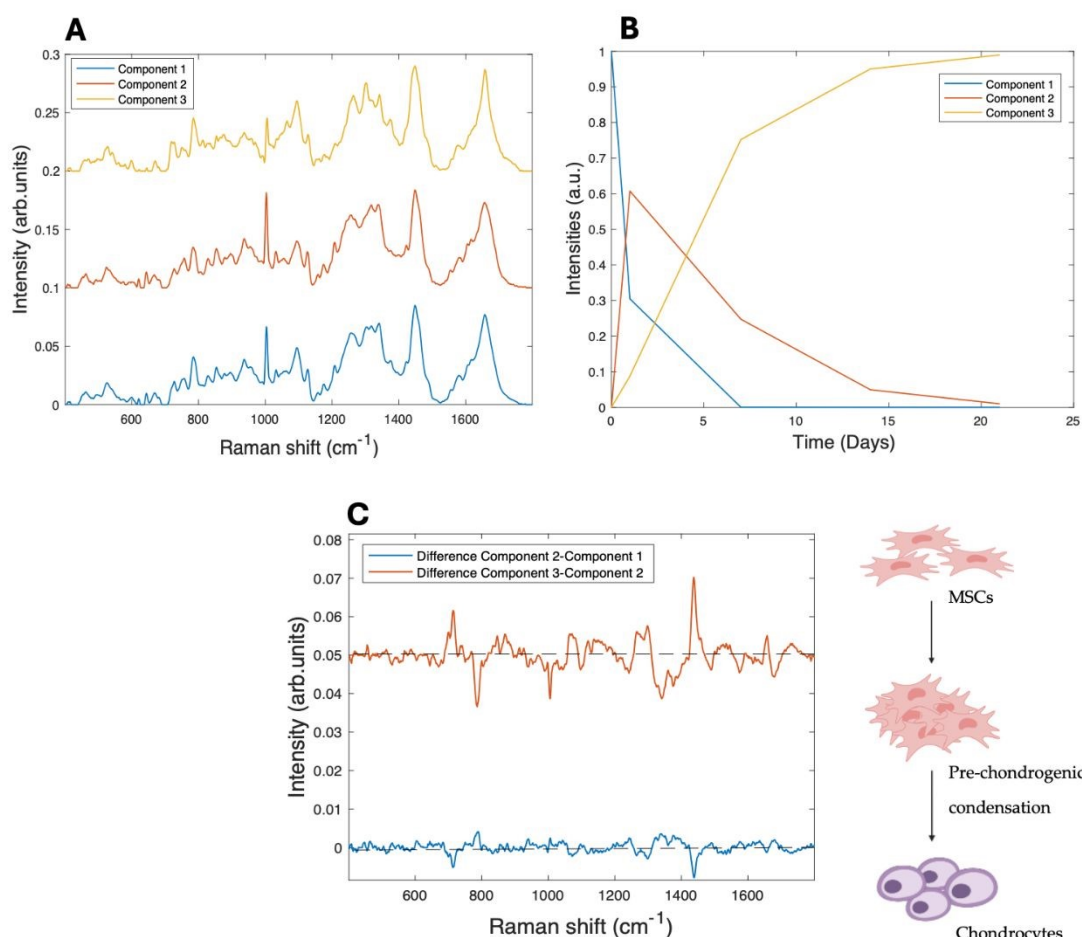


Figure 3. **A)** Raman spectra of the resolved components corresponding to cytoplasm for 21 days of differentiation on 3D collagen I hydrogels. **B)** Three stage kinetic model of the evolution of the kinetic components $A \rightarrow B$, $B \rightarrow C$. **C)** Difference spectra between the first and the second component (blue) and second and third (red).

Figure 3 illustrates the kinetic profile of the third observed subcellular region, the cytoplasm. The observation of the cytoplasmic features, alongside those from the nucleolus, provides a comprehensive picture of the dynamic biochemical changes occurring during chondrocyte



differentiation. As was the case for the other cellular regions, singular value decomposition (SVD) of the data allowed for the identification of three spectral components. In the kinetic analysis, Component 1 is seen to rapidly decay at a rate of $k_1 = 1.2 \pm 0.2$ per day, while, in contrast to the other cellular regions, Component 2 also decays rapidly, such that Component 3 completely dominates after 21 days. In fact, examination of the spectra of Component 1 and 2 indicates a high degree of similarity, and the difference spectrum of Figure 3.C is relatively weak. It could therefore be considered that the evolution of the cytoplasmic region, in the cells grown on the 3D hydrogel matrix, is better described by a two stage process $A \rightarrow B$, at a single rate k_1 .

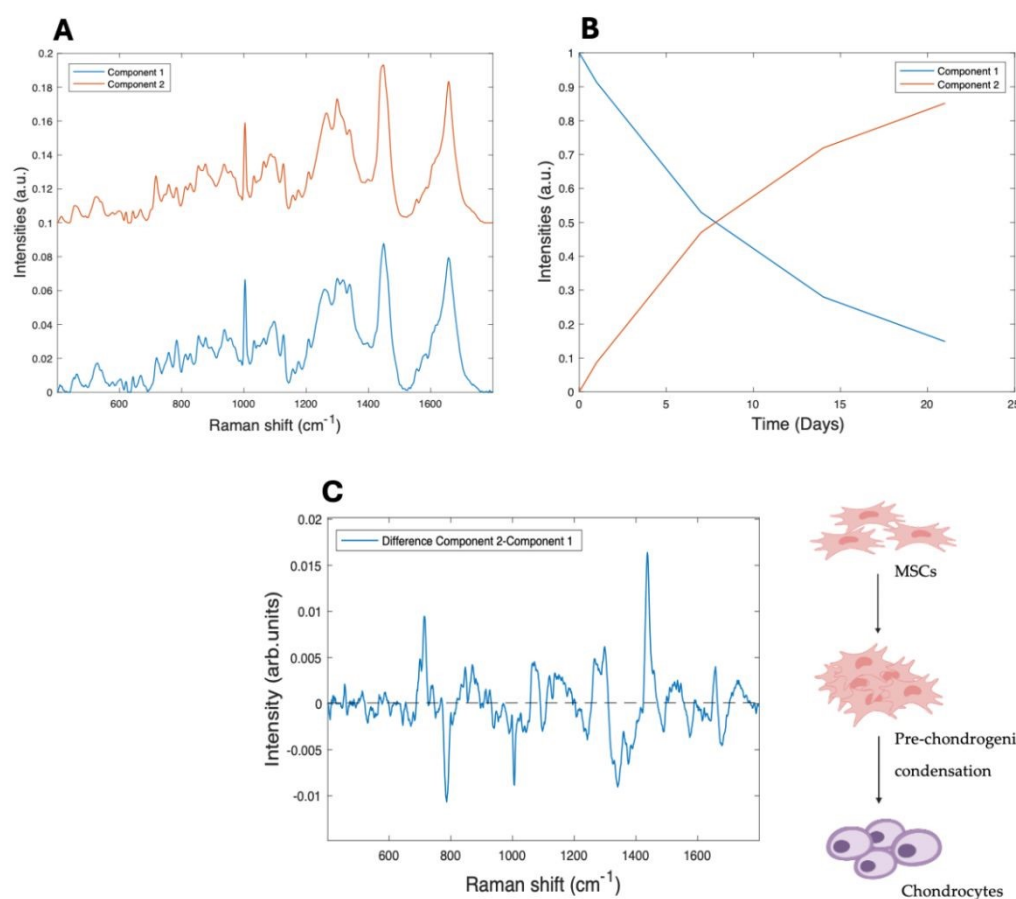


Figure 4. **A)** Raman spectra of the resolved components corresponding to cytoplasm for 21 days of differentiation on 3D collagen I hydrogels. **B)** Two stage kinetic model of the

1 evolution of the kinetic components A \rightarrow B. C) Difference spectrum between the first and the
2 second component (blue).
3
4
5
6
7
8
9

10 Figure 4 illustrates the results of the analysis of the spectroscopic data of the cytoplasm on 3D
11 substrates according to a two stages kinetic model A \rightarrow B. Component 1 decays almost
12 completely over the 21 day period, while Component 2 increases concomitantly to a value of
13 ~ 0.85 . Figure 4.C shows the main observed peaks, associated with amide II (1257 cm^{-1}), and
14 lipids (1300 cm^{-1}), $\sim 1314\text{-}21\text{ cm}^{-1}$ CH_3CH_2 twisting (collagen assignment) and suggests that
15 the initiation of extracellular matrix formation is observed in the transition from the first to the
16 second component (figure 3.B) [50, 63]. More prominent peaks in the spectrum include those
17 at $\sim 1290\text{-}1400\text{ cm}^{-1}$ and $\sim 840\text{-}860\text{ cm}^{-1}$, corresponding to CH bending and the C-O-C group
18 of polysaccharides, $\sim 1266\text{ cm}^{-1}$, $\sim 1314\text{-}21\text{ cm}^{-1}$, 1335 cm^{-1} , 1342 cm^{-1} corresponding to
19 CH_3CH_2 contributions of collagen, amide III and glycosaminoglycans (GAGs) respectively,
20 the essential building blocks of the chondrogenic matrix [49, 52, 53, 64].
21
22
23
24
25
26
27
28
29
30
31
32
33
34
35
36
37
38
39
40
41
42

43 In such a 2 stage model, the rate of change, k_1 , is determined to be 0.16 ± 0.02 per day. Analysis
44 of the data for differentiation on a 2D substrate fit well to a 3 Component model, with $k_1 = 0.15$
45 ± 0.01 per day, $k_2 = 0.049 \pm 0.005$ per day.
46
47
48
49
50
51
52
53
54
55
56
57
58
59
60

3.2. Discussion

44 The approach explored in this work enables the observation of molecular evolution without
45 perturbing the system, making it invaluable for studying dynamic cellular processes. While
46 biochemical based assays can establish the presence of specific biomarkers of the progression
47 of the differentiation process at fixed points in time, RMS analysis monitors the progression in
48 a more holistic fashion, shedding more light on the process subcellularly, as well as within the
49 cell population. By offering non-destructive, label-free insights at both cellular and
50 extracellular levels, RMS provides a comprehensive view of biochemical transitions occurring
51
52
53
54
55
56
57
58
59
60



1
2
3 during chondrogenesis and cartilage formation [65-67]. Importantly, RMS has further View Article Online
DOI: 10.1039/D4AN01509F

4
5 demonstrated its capacity to distinguish between different stages of chondrogenesis by
6
7 detecting key biochemical changes, including the synthesis and organisation of crucial ECM
8
9 components [33, 34, 68, 69]. A key advantage of RMS resides in its ultimate capacity for real-
10
11 time, monitoring of biochemical alterations during chondrogenesis, thereby providing a
12
13 dynamic and continuous assessment that contrasts with the fixed time-point data obtained from
14
15 conventional biochemical assays. Additionally, it facilitates the detection of a broad range of
16
17 extracellular matrix (ECM) constituents, encompassing both sulphated and non-sulphated
18
19 glycosaminoglycans (GAGs). This capability distinguishes it from dye-based assays, such as
20
21 Blyscan and Alcian Blue, which exhibit selectivity towards sulphated GAGs, by affording a
22
23 more comprehensive molecular characterisation of the differentiating tissue [19, 64]. The
24
25 combination of RMS with multivariate curve resolution-alternating least squares (MCR-ALS)
26
27 represents a significant advancement in extracting kinetic data from complex biological
28
29 systems [36]. By quantifying dynamic cellular composition changes over time, this technique
30
31 offers valuable insights into the biochemical signatures of chondrogenesis at the single-cell
32
33 level. While similar techniques have been used before, this study presents a novel application
34
35 by integrating these methods for real-time monitoring of subcellular progression during
36
37 chondrogenesis, offering a more nuanced and comprehensive analysis compared to traditional
38
39 methods. Kinetic studies have previously described the biphasic nature of chondrogenesis, with
40
41 distinct ECM production phases [70, 71].

42
43
44
45
46
47
48
49 Sorrell *et al.* (2018) investigated the kinetics of chondrogenesis in hMSC-derived aggregates
50
51 at defined time points and used microarray analysis to monitor time-dependent mRNA
52
53 expression profiles of ECM-related genes, including early markers like PAPSS2, PRG4, and
54
55 fibronectin, and later cartilage-specific genes such as COL2A1 and ACAN [71]. These data
56
57 revealed the biphasic pattern in which early matrix production involved fibrous proteins and
58
59
60

1
2
3 small proteoglycans, followed by later accumulation of cartilage-specific ECM components [71].
4
5
6
7

8 This dynamic pattern of ECM regulation aligns with the findings presented, providing a
9
10 valuable framework for understanding the temporal regulation of ECM synthesis during
11
12 cartilage differentiation. In addition, a recent study applied RMS combined with MCR-ALS to
13
14 monitor biochemical changes in chondrocytes during osteoarthritis progression, focusing on
15
16 apoptotic processes at the single-cell level. The study highlighted how MCR-ALS can
17
18 deconvolve complex Raman spectra to isolate molecular components like lipids, DNA, and
19
20 proteins, assessing their relative changes in response to OA-induced degeneration [72]. By
21
22 applying this approach to both two-dimensional (2D) and three-dimensional (3D) culture
23
24 systems [40], the investigation reveals notable differences in the pace and pattern of
25
26 differentiation. While the initial study indicated that the cytoplasmic regions displayed a
27
28 distinct behaviour compared to the nuclear regions, the comparative study of the differentiation
29
30 process in a 3D culture environment compared to the 2D culture, further indicated that the
31
32 differentiation process overall was more rapid in the 3D environment [40]. The application of
33
34 MCR-ALS enables a more quantitative approach to the analysis of the progression of the
35
36 differentiation process, as well as a quantitative comparison of the progression in different cell
37
38 culture environments, in terms of the rate constants of the different kinetic stages [38]. The
39
40 optical resolution of Raman microspectroscopy furthermore enables a quantitative comparison
41
42 of the progression rates within the different subcellular regions, in this study, the nucleolus,
43
44 nucleus and cytoplasmic regions, which may lay the foundation for an improved understanding
45
46 of the differentiation and condensation process.
47
48
49
50
51
52

53 The analysis indicates that the nucleolus and the nucleus are the primary sites of biochemical
54
55 activity during chondrogenesis, significant spectral changes being observed early in the
56
57 differentiation process, while the cytoplasm is a direct manifestation of those changes, and
58
59
60

Downloaded on 08 May 2025 at 08:59 AM.
This article is licensed under a Creative Commons Attribution 3.0 Unported Licence.
View Article Online
DOI: 10.1039/D4AN01509F



1
2
3 region in which the extracellular matrix is generated. In both 3D and 2D culture environments,
4 the initial rate of change of the nucleolar region is highest, followed by the surrounding nuclear
5 regions. In the 2D culture, the rate of subsequent evolution of the cytoplasmic region appears
6 to be similar to that of the nuclear region, while in the 3D culture environment, the condensation
7 stage associated with the growth of the extracellular matrix appears to begin from the outset.
8 Notably, a similar difference was observed in the evolution of the condensation pellet in 2D
9 and 3D [40], whereby a progressive evolution of the pellet from the edges to the centre was
10 observed in 2D, whereas a much more spatially uniform evolution was observed in the 3D
11 environment. This is consistent with the earlier deposition of the extracellular matrix in the 3D
12 environment, potentially prompted by the biocompatible nature of the collagen hydrogel.
13
14 The MCR-ALS analysis is thus a promising analytic tool to quantify the kinetics of the
15 evolution of the differentiation process, and also to identify the specific biochemical signatures
16 at the different stages. It is noted, however, that the dataset should be considered sparse, in that
17 the measurement intervals are relatively long compared to the differentiation stages, and the
18 process has not been completed by the stage of the last measurement, at 21 days. With the
19 exception of Component A at $t=0$, there is considerable overlap of all components at all other
20 measurement times, and thus the analysis is subject to ambiguity and essentially has difficulty
21 in completely unmixing the components [73]. This is potentially the reason for the near mirror
22 image nature of the difference spectra in Figures 1.2 & 3.C, which could be improved by more
23 regular, ultimately real-time sampling over the full time course. Nevertheless, the study
24 demonstrates the potential benefits of kinetic monitoring of the label free spectroscopic
25 signatures of the differentiation process at a subcellular and cell population level.
26
27 Growth conditions represent a critical determinant in directing mesenchymal stem cell (MSC)
28 chondrogenesis, and therefore the differentiation rates. The complex interplay between cell
29 confluence, three-dimensional architecture, and substrate porosity orchestrates both the
30

biochemical and mechanical cues necessary for differentiation [3, 4, 74]. The significance of microenvironmental modifications accompanying the differentiation of MSCs into chondrocytes has been extensively investigated [75]. Changes in the extracellular matrix (ECM), shaped by the synthesis and remodelling of its components, are crucial for successful chondrogenesis, as evidenced by a marked upregulation of collagen type II and ACAN, alterations in collagen type I, and increased synthesis of proteoglycans and glycoproteins during chondrogenic differentiation. The density at which MSCs are cultured can influence gene expression, proliferation behaviour, and overall morphology [76]. High confluence not only promotes a rounded cell morphology, an essential feature of chondrocyte-like behaviour, but also significantly enhances the synthesis of cartilage-specific ECM proteins, such as collagen type II and aggrecan, through increased cell-to-cell interactions and mechanical cues [77]. Moreover, the role of optimised high-density, three-dimensional (3D) culture conditions in promoting chondrogenesis has been widely explored [10, 15, 78-82]. Three-dimensional culture systems exhibit elevated expression of chondrogenic markers such as COL2A1, SOX9, and ACAN, which are minimally expressed in two-dimensional (2D) monolayers. In contrast, hypertrophic markers, including COL10A1, RUNX2, and ALP, are significantly upregulated in 2D cultures but suppressed in 3D environments [78, 82-84]. Glycosaminoglycan (GAG) content has been reported to be significantly higher in 3D cultures, whereas cell proliferation is predominantly observed in 2D systems, suggesting divergent pathways that favour matrix production versus cellular expansion, respectively.

4. Conclusions

This study demonstrates the efficacy of Raman microspectroscopy (RMS) as a powerful tool for *in situ* monitoring and potentially quality process control of cell-based therapies. Using the model example of chondrogenesis from mesenchymal stem cells, *in vitro*, the sequential biochemical changes in the nucleolar, nuclear and cytoplasmic regions can be identified. MCR-

ALS analysis of Raman spectra furthermore provides detailed insights into the biochemical changes underlying this process, allowing for the identification of specific molecular markers and the quantification of their relative contributions and evolution rates.

The study seeks to address the limitations of conventional fixed-timepoint assays, such as immunostaining, PCR, or histological analysis, which require destructive sample preparation and provide only a static view of cellular processes at a single time point. This inherently restricts their capacity to track dynamic changes and transient biochemical states throughout differentiation. In contrast, Raman microspectroscopy allows non-invasive, real-time monitoring of the same sample, thereby enabling continuous observation of molecular evolution and offering a detailed kinetic profile of chondrogenesis over time.

The analysis confirms that the differentiation process is initiated in the nucleolar regions, before progressing in the nuclear and cytoplasmic regions. The analysis also proves that the process is more rapid in cell cultures grown on the 3D collagen hydrogel environment, than those on the 2D substrate. This non-destructive and sensitive technique, therefore, offers a valuable approach for studying cellular differentiation and optimising culture conditions for tissue engineering applications. By combining Raman microspectroscopy and MCR-ALS, researchers can gain a deeper understanding of the complex mechanisms involved in chondrogenesis and develop more effective strategies for regenerative medicine.

Acknowledgements

FR acknowledges financial support from the TU Dublin Fiosraigh Postgraduate Scholarship programme.

Conflicts of Interests

There are no conflicts to declare.

5. References

1. Rangan, S., et al., *Applications of Raman spectroscopy in the development of cell therapies: state of the art and future perspectives*. Analyst, 2020. **145**(6): p. 2070-2105.
2. Richardson, S.M., et al., *Mesenchymal stem cells in regenerative medicine: Focus on articular cartilage and intervertebral disc regeneration*. Methods (San Diego, Calif.), 2016. **99**: p. 69-80.
3. Tacchetti, C., et al., *Cell condensation in chondrogenic differentiation*. Experimental cell research, 1992. **200**(1): p. 26-33.
4. Hall, B.K. and T. Miyake, *Divide, accumulate, differentiate: cell condensation in skeletal development revisited*. Int J Dev Biol, 1995. **39**(6): p. 881-93.
5. Hall, B.K. and T. Miyake, *The membranous skeleton: the role of cell condensations in vertebrate skeletogenesis*. Anatomy and Embryology, 1992. **186**(2): p. 107-124.
6. Owida, H.A., et al., *Vibrational spectroscopic monitoring and biochemical analysis of pericellular matrix formation and maturation in a 3-dimensional chondrocyte culture model*. Analyst, 2018. **143**(24): p. 5979-5986.
7. Doyle, A.D., *Generation of 3D Collagen Gels with Controlled Diverse Architectures*. Curr. Protoc. Cell Biol., 2016(1934-2616).
8. Moulisová, V., et al., *Hybrid Protein-Glycosaminoglycan Hydrogels Promote Chondrogenic Stem Cell Differentiation*. ACS Omega, 2017(2470-1343): p. 7609–7620.
9. Yang, J., et al., *The negatively charged microenvironment of collagen hydrogels regulates the chondrogenic differentiation of bone marrow mesenchymal stem cells in vitro and in vivo*. J Mater Chem B, 2020. **8**(2050-7518): p. 4680-4693.
10. Nöth, U., et al., *Chondrogenic differentiation of human mesenchymal stem cells in collagen type I hydrogels*. J Biomed Mater Res A, 2007. **83**(3): p. 626-35.
11. Ghosh, S., M. Laha, and S. Mondal, Sengupta, S., & Kaplan, D. L., *In vitro model of mesenchymal condensation during chondrogenic development*. Biomaterials, 2009. **30**: p. 6530–6540.
12. Grassel, S., S. Stöckl, and Z. Jenei-Lanzl, *Isolation, culture, and osteogenic/chondrogenic differentiation of bone marrow-derived mesenchymal stem cells*, in *Methods Mol Biol*. 2012. p. 203-67.

- 1
2
3
4
5
6
7
8
9
10
11
12
13
14
15
16
17
18
19
20
21
22
23
24
25
26
27
28
29
30
31
32
33
34
35
36
37
38
39
40
41
42
43
44
45
46
47
48
49
50
51
52
53
54
55
56
57
58
59
60
13. Lefebvre, V., et al., *SOX9 is a potent activator of the chondrocyte-specific enhancer of the pro alpha1(II) collagen gene*. Mol Cell Biol, 1997. **17**(4): p. 2336-46. View Article Online
DOI: 10.1037/D4AN01509F
14. Akiyama, H., et al., *The transcription factor Sox9 has essential roles in successive steps of the chondrocyte differentiation pathway and is required for expression of Sox5 and Sox6*. Genes Dev, 2002. **16**(0890-9369): p. 2813-28.
15. Miao, Z., et al., *Collagen, agarose, alginate, and Matrigel hydrogels as cell substrates for culture of chondrocytes in vitro: A comparative study*. J Cell Biochem, 2018. **119**(10): p. 7924-7933.
16. Schwarzl, T., et al., *Transcriptional profiling of early differentiation of primary human mesenchymal stem cells into chondrocytes*. Scientific Data, 2023. **10**.
17. Solursh, M., T.F. Linsenmayer, and K.L. Jensen, *Chondrogenesis from single limb mesenchyme cells*. Developmental Biology, 1982. **94**(1): p. 259-264.
18. Solchaga, L.A., K.J. Penick, and J.F. Welter, *Chondrogenic differentiation of bone marrow-derived mesenchymal stem cells: tips and tricks*. Methods in molecular biology (Clifton, N.J.), 2011. **698**: p. 253-278.
19. Mohamed, H.T., et al., *Implementation of infrared and Raman modalities for glycosaminoglycan characterization in complex systems*. Glycoconjugate Journal, 2017. **34**(3): p. 309-323.
20. Grässel, S., et al., *Gene and protein expression profile of naive and osteo-chondrogenically differentiated rat bone marrow-derived mesenchymal progenitor cells*. International Journal of Molecular Medicine 2009. **23**(6): p. 745-755.
21. Ahmed, N., et al., *CD45-positive cells of haematopoietic origin enhance chondrogenic marker gene expression in rat marrow stromal cells*. International Journal of Molecular Medicine, 2006. **18**(2): p. 233-240.
22. Xia, Y., E.M. Darling, and W. Herzog, *Functional properties of chondrocytes and articular cartilage using optical imaging to scanning probe microscopy*. J Orthop Res, 2018. **36**(2): p. 620-631.
23. Fernández-Iglesias, Á., et al., *A simple method based on confocal microscopy and thick sections recognizes seven subphases in growth plate chondrocytes*. Sci Rep, 2020. **10**(1): p. 6935.
24. Aigner, J., et al., *Distribution and viability of cultured human chondrocytes in a three-dimensional matrix as assessed by confocal laser scan microscopy*. In Vitro Cell Dev Biol Anim, 1997. **33**(6): p. 407-9.

- 1
2
3
4
5
6
7
8
9
10
11
12
13
14
15
16
17
18
19
20
21
22
23
24
25
26
27
28
29
30
31
32
33
34
35
36
37
25. Walter, I., et al., *Confocal laser scanning microscopy of chondrocytes in vitro: cytoskeletal changes after quinolone treatment*. Scanning, 1998. **20**(7): p. 511-5.
26. Zayed, M., et al., *Donor-Matched Comparison of Chondrogenic Potential of Equine Bone Marrow- and Synovial Fluid-Derived Mesenchymal Stem Cells: Implications for Cartilage Tissue Regeneration*. Front Vet Sci, 2016. **3**: p. 121.
27. Lin, Y., et al., *Chemical analysis of single cells*. Anal Chem, 2011. **83**(12): p. 4369-92.
28. Bour-Dill, C., et al., *Determination of intracellular organelles implicated in daunorubicin cytoplasmic sequestration in multidrug-resistant MCF-7 cells using fluorescence microscopy image analysis*. Cytometry, 2000. **39**(1): p. 16-25.
29. Ghita, A., et al., *Applications of Raman micro-spectroscopy to stem cell technology: label-free molecular discrimination and monitoring cell differentiation*. EPJ Tech Instrum, 2015. **2**(1): p. 6.
30. Murdoch, A.D., et al., *Chondrogenic differentiation of human bone marrow stem cells in transwell cultures: generation of scaffold-free cartilage*. Stem Cells, 2007. **25**(11): p. 2786-96.
31. Byrne, H.J., et al., *Spectroscopy for the next generation: quo vadis?* Analyst, 2015. **140**(7): p. 2066-73.
32. Baker, M.J., et al., *Clinical applications of infrared and Raman spectroscopy: state of play and future challenges*. Analyst, 2018. **143**(8): p. 1735-1757.
33. Ravera, F., E. Efeoglu, and H.J. Byrne, *Monitoring stem cell differentiation using Raman microspectroscopy: chondrogenic differentiation, towards cartilage formation*. Analyst, 2021(1364-5528): p. 322-337.
34. Lazarevic, J.J., et al., *Probing primary mesenchymal stem cells differentiation status by micro-Raman spectroscopy*. Spectrochim Acta A Mol Biomol Spectrosc, 2019. **213**: p. 384-390.
35. de Juan, A. and R. Tauler, *Chemometrics applied to unravel multicomponent processes and mixtures: Revisiting latest trends in multivariate resolution*. Analytica Chimica Acta, 2003. **500**(1-2): p. 195-210.
36. Felten, J., et al., *Vibrational spectroscopic image analysis of biological material using multivariate curve resolution-alternating least squares (MCR-ALS)*. 217-40, 2015. **10**(1750-2799 (Electronic)): p. 217-40.
37. de Juan, A., J. Jaumot, and R. Tauler, *Multivariate Curve Resolution (MCR). Solving the mixture analysis problem*. Analytical Methods, 2014. **6**: p. 4964-4976.

- 1
2
3
4
5
6
7
8
9
10
11
12
13
14
15
16
17
18
19
20
21
22
23
24
25
26
27
28
29
30
31
32
33
34
35
36
37
38
39
40
41
42
43
44
45
46
47
48
49
50
51
52
53
54
55
56
57
58
59
60
38. Pérez-Guaita, D., et al., *Combining Pharmacokinetics and Vibrational Spectroscopy MCR-ALS Hard-and-Soft Modelling of Drug Uptake In Vitro Using Tailored Kinetic Constraints*. . 2022. **11**: p. 1555. View Article Online
DOI: 10.1039/D1AN01509F
39. Matveeva, I., et al., *Multivariate Curve Resolution Alternating Least Squares Analysis of In Vivo Skin Raman Spectra*. *Sensors*, 2022. **22**: p. 9588.
40. Ravera, F., E. Efeoglu, and H.J. Byrne, *A comparative analysis of stem cell differentiation on 2D and 3D substrates using Raman microspectroscopy*. *The Analyst*, 2024. **149**(15): p. 4041–4053.
41. Sangeetha, P., et al., *Mesenchymal stem cells derived from rat bone marrow (rbm msc): techniques for isolation, expansion and differentiation*. *Journal of Stem Cell Research & Therapeutics*, 2017. **3**(3): p. 272-277.
42. Lotfy, A., et al., *Comparative study of biological characteristics of mesenchymal stem cells isolated from mouse bone marrow and peripheral blood*. *Biomed Rep*, 2019. **11**(4): p. 165-170.
43. Zhang, H., et al., *The ability to form cartilage of NPMSC and BMSC in SD rats*. *Int J Clin Exp Med*, 2015. **8**(4): p. 4989-96.
44. Bonnier, F., et al., *In vitro analysis of immersed human tissues by Raman microspectroscopy*. *Journal of Raman Spectroscopy*, 2011. **42**(5): p. 888-896.
45. Bonnier, F., et al., *Analysis of human skin tissue by Raman microspectroscopy: Dealing with the background*. *Vibrational Spectroscopy*, 2012. **61**: p. 124-132.
46. Boyack, R. and E.C. Le Ru, *Investigation of particle shape and size effects in SERS using T-matrix calculations*. *Phys Chem Chem Phys*, 2009. **11**(34): p. 7398-405.
47. Kerr, L.T. and B.M. Hennelly, *A multivariate statistical investigation of background subtraction algorithms for Raman spectra of cytology samples recorded on glass slides*. *Chemometrics and Intelligent Laboratory Systems*, 2016. **158**: p. 61-68.
48. Jaumot, J., et al., *A graphical user-friendly interface for MCR-ALS: a new tool for multivariate curve resolution in MATLAB*. *Chemometrics and Intelligent Laboratory Systems*, 2005. **76**(1): p. 101-110.
49. Liu, Z., et al., *Circulation and long-term fate of functionalized, biocompatible single-walled carbon nanotubes in mice probed by Raman spectroscopy*. *Proc Natl Acad Sci U S A*, 2008. **105**: p. 1410-5.
50. Chan, J.W., et al., *Micro-Raman spectroscopy detects individual neoplastic and normal hematopoietic cells*. *Biophys J*, 2006. **90**(2): p. 648-56.

- 1
2
3
4
5
6
7
8
9
10
11
12
13
14
15
16
17
18
19
20
21
22
23
24
25
26
27
28
29
30
31
32
33
34
35
36
37
38
39
40
41
42
43
44
45
46
47
48
49
50
51
52
53
54
55
56
57
58
59
60
51. Stone, N., et al., *Raman spectroscopy for identification of epithelial cancers*, Faraday Discuss, 2004. **126**: p. 141-57; discussion 169-83. View Article Online
DOI: 10.1039/B4AN01509F
52. Talari, A.C.S., et al., *Raman Spectroscopy of Biological Tissues*. Applied Spectroscopy Reviews, 2014. **50**(1): p. 46-111.
53. Bonnier, F. and H.J. Byrne, *Understanding the molecular information contained in principal component analysis of vibrational spectra of biological systems*. Analyst, 2012. **137**(2): p. 322-32.
54. Huang, Z., et al., *Near-infrared Raman spectroscopy for optical diagnosis of lung cancer*. Proc Natl Acad Sci U S A, 2003. **107**(0020-7136): p. 1047-52.
55. Notingher, I. and I. Bisson, Anne E.Randle, Wesley L.Polak, Julia M. P. Hench, Larry L., *In situ spectroscopic study of nucleic acids in differentiating embryonic stem cells*. Vibrational Spectroscopy, 2004. **35**(1): p. 199 - 203.
56. Seibel, M.J., S.P. Robins, and J.P. Bilezikian, *Dynamics of Bone and Cartilage Metabolism*. 2nd ed. Principles and Clinical Applications. 2006: Elsevier.
57. Chen, H., et al., *Runx2 regulates endochondral ossification through control of chondrocyte proliferation and differentiation*. J Bone Miner Res . 2014(1523-4681).
58. Rocha, B., et al., *Characterization of lipidic markers of chondrogenic differentiation using mass spectrometry imaging*. Proteomics, 2015. **15**(4): p. 702-13.
59. Hall, B.K. and T. Miyake, *All for one and one for all: condensations and the initiation of skeletal development*. BioEssays : news and reviews in molecular, cellular and developmental biology, 2000. **22**(2): p. 138-147.
60. Jyothi Lakshmi, R., et al., *Tissue Raman spectroscopy for the study of radiation damage: brain irradiation of mice*. Radiation research, 2002. **157**: p. 175-82.
61. Mainreck, N., et al., *Rapid characterization of glycosaminoglycans using a combined approach by infrared and Raman microspectroscopies*. J Pharm Sci, 2011. **100**(2): p. 441-50.
62. Ellis, R., E. Green, and C.P. Winlove, *Structural Analysis of Glycosaminoglycans and Proteoglycans by Means of Raman Microspectrometry*. Connective Tissue Research, 2009. **50**(1): p. 29-36.
63. Dukor, R.K., *Vibrational Spectroscopy in the Detection of Cancer*, in *Handbook of Vibrational Spectroscopy*, J.M. Chalmers and P.R. Griffiths, Editors. 2006, J.M. Chalmers and P.R. Griffiths: Handbook of Vibrational Spectroscopy.

- 1
2
3
4
5
6
7
8
9
10
11
12
13
14
15
16
17
18
19
20
21
22
23
24
25
26
27
28
29
30
31
32
33
34
35
36
37
38
39
40
41
42
43
44
45
46
47
48
49
50
51
52
53
54
55
56
57
58
59
60
64. Brézillon, S., et al., *Probing glycosaminoglycan spectral signatures in live cells and their conditioned media by Raman microspectroscopy*. Analyst, 2017. **142**: p. 1333-1341. View Article Online
DOI: 10.1039/D4AN01509F
65. Bergholt, M.S., A. Serio, and M.B. Albro, *Raman Spectroscopy: Guiding Light for the Extracellular Matrix*. Front Bioeng Biotechnol, 2019. **7**: p. 303.
66. Bergholt, M.S., et al., *Raman Spectroscopy Reveals New Insights into the Zonal Organization of Native and Tissue-Engineered Articular Cartilage*. ACS Cent Sci, 2016. **2**(12): p. 885-895.
67. Albro, M.B., et al., *Raman spectroscopic imaging for quantification of depth-dependent and local heterogeneities in native and engineered cartilage*. NPJ Regen Med, 2018. **3**: p. 3.
68. Bonifacio, A., et al., *Chemical imaging of articular cartilage sections with Raman mapping, employing uni- and multi-variate methods for data analysis*. Analyst, 2010. **135**(12): p. 3193–3204.
69. Moura, C.C., et al., *Raman spectroscopy and coherent anti-Stokes Raman scattering imaging: prospective tools for monitoring skeletal cells and skeletal regeneration*. J R Soc Interface, 2016. **13**(118).
70. Sekiya, I., et al., *In vitro cartilage formation by human adult stem cells from bone marrow stroma defines the sequence of cellular and molecular events during chondrogenesis*. Proc Natl Acad Sci U S A, 2002. **99**(7): p. 4397-402.
71. Sorrell, J.M., R.A. Somoza, and A.I. Caplan *Human mesenchymal stem cells induced to differentiate as chondrocytes follow a biphasic pattern of extracellular matrix production*. Inc. J Orthop Res, 2018. **36**(6): p. 1757-1766.
72. Uppal, G., et al., *Unravelling changes in single-cell osteoarthritic chondrocytes through coupling of Raman spectroscopy and multivariate curve resolution-alternating least square (MCR-ALS) algorithm*. Microchemical Journal, 2025. **212**: p. 113264.
73. de Juan, A.M., M. Martínez, M. Tauler, R., *Combining hard- and soft-modelling to solve kinetic problems*. Chemometrics and Intelligent Laboratory Systems, 2000. **54**(2): p. 123-141.
74. Lee, Y.S. and C.M. Chuong, *Adhesion molecules in skeletogenesis: I. Transient expression of neural cell adhesion molecules (NCAM) in osteoblasts during endochondral and intramembranous ossification*. J Bone Miner Res, 1992. **7**(12): p. 1435-46.

- 1
2
3
4
5
6
7
8
9
10
11
12
13
14
15
16
17
18
19
20
21
22
23
24
25
26
27
28
29
30
31
32
33
34
35
36
37
38
39
40
41
42
43
44
45
46
47
48
49
50
51
52
53
54
55
56
57
58
59
60
75. Djouad, F., et al., *Microenvironmental changes during differentiation of mesenchymal stem cells towards chondrocytes*. *Arthritis Res Ther*, 2007. **9**(2). View Article Online
DOI: 10.1039/B4AN01509F
76. Bean, A.C. and R. Tuan, *Fiber diameter and seeding density influence chondrogenic differentiation of mesenchymal stem cells seeded on electrospun poly(ϵ -caprolactone) scaffolds*. *Biomedical Materials*, 2015. **10**.
77. Zhang, L.S., P.Xu, C. Yu, W. Huang, D., *Chondrogenic differentiation of human mesenchymal stem cells: a comparison between micromass and pellet culture systems*. *Biotechnol Lett* 2010. **32**(9): p. 1339.
78. Caron, M.M.J., et al., *Redifferentiation of dedifferentiated human articular chondrocytes: comparison of 2D and 3D cultures*. *Osteoarthritis and cartilage*, 2012. **20**(10): p. 1170-1178.
79. Wang, T. and F. Yang, *A comparative study of chondroitin sulfate and heparan sulfate for directing three-dimensional chondrogenesis of mesenchymal stem cells*. *Stem Cell Research and Therapy*, 2017. **8**(1757-6512).
80. Naito, H., et al., *The advantages of three-dimensional culture in a collagen hydrogel for stem cell differentiation*. *J Biomed Mater Res A.*, 2013. **10**(1552-4965): p. 2838-45.
81. Jin, G.Z. and H.W. Kim, *Effects of Type I Collagen Concentration in Hydrogel on the Growth and Phenotypic Expression of Rat Chondrocytes*. *Tissue Eng Regen Med*, 2017. **14**(4): p. 383-391.
82. Bosnakovski, D., et al., *Chondrogenic differentiation of bovine bone marrow mesenchymal stem cells (MSCs) in different hydrogels: influence of collagen type II extracellular matrix on MSC chondrogenesis*. *Biotechnol Bioeng*, 2006(0006-3592): p. 1152-63.
83. Bhardwaj, N. and C.K. Subhas, *Chondrogenic differentiation of rat MSCs on porous scaffolds of silk fibroin/chitosan blends*. *Biomaterials*, 2012. **33**(10): p. 2848-2857.
84. Takeda, S., et al., *Continuous expression of *Cbfa1* in nonhypertrophic chondrocytes uncovers its ability to induce hypertrophic chondrocyte differentiation and partially rescues *Cbfa1*-deficient mice*. *Genes Dev*, 2001. **15**(4): p. 467-81.

Data Availability Statement

The data that support the findings of this study are available from the corresponding author
Francesca Ravera, (D16126527@mytudublin.ie) upon request.

Signed _____ *Francesca Ravera* Date _____ 4-12-2024

Analyst Accepted Manuscript

1
2
3
4
5
6
7
8
9
10
11
12
13
14
15
16
17
18
19
20
21
22
23
24
25
26
27
28
29
30
31
32
33
34
35
36
37
38
39
40
41
42
43
44
45
46
47
48
49
50
51
52
53
54
55
56
57
58
59
60

Open Access Article. Published on 08 May 2025. Downloaded on 06/11/2025 5:08:59 AM.
This article is licensed under a Creative Commons Attribution 3.0 Unported Licence.

